Cell

Motor Deficit in a *Drosophila* Model of Mucolipidosis Type IV due to Defective Clearance of Apoptotic Cells

Kartik Venkatachalam,[1] A. Ashleigh Long,[2] Rebecca Elsaesser,[1] Daria Nikolaeva,[1] Kendal Broadie,[2] and Craig Montell[1,*]
[1]Departments of Biological Chemistry and Neuroscience, Center for Sensory Biology, The Johns Hopkins University School of Medicine, Baltimore, MD 21205, USA
[2]Department of Biological Sciences, Vanderbilt Brain Institute, Kennedy Center for Research on Human Development, Vanderbilt University, Nashville, TN 37232, USA
*Correspondence: cmontell@jhmi.edu
DOI 10.1016/j.cell.2008.09.041

SUMMARY

Disruption of the Transient Receptor Potential (TRP) mucolipin 1 (TRPML1) channel results in the neurodegenerative disorder mucolipidosis type IV (MLIV), a lysosomal storage disease with severe motor impairments. The mechanisms underlying MLIV are poorly understood and there is no treatment. Here, we report a *Drosophila* MLIV model, which recapitulates the key disease features, including abnormal intracellular accumulation of macromolecules, motor defects, and neurodegeneration. The basis for the buildup of macromolecules was defective autophagy, which resulted in oxidative stress and impaired synaptic transmission. Late-apoptotic cells accumulated in *trpml* mutant brains, suggesting diminished cell clearance. The accumulation of late-apoptotic cells and motor deficits were suppressed by expression of *trpml*$^+$ in neurons, glia, or hematopoietic cells. We conclude that the neurodegeneration and motor defects result primarily from decreased clearance of apoptotic cells. Since hematopoietic cells in humans are involved in clearance of apoptotic cells, our results raise the possibility that bone marrow transplantation may limit the progression of MLIV.

INTRODUCTION

The Transient Receptor Potential (TRP) channel superfamily participates in a remarkable diversity of processes in the nervous system (Venkatachalam and Montell, 2007). Nevertheless, the only neurodegenerative disease linked to a TRP channel is the early childhood disorder, mucolipidosis IV (MLIV). This highly debilitating, autosomal recessive disease is characterized by severe motor deficits, mental retardation, and neurodegeneration, including retinal degeneration (Bach, 2005). MLIV is a lysosomal storage disorder (LSD), 1 of ~40 LSDs, which together represent the most common cause of neurodegeneration during childhood (Cooper, 2003). As is typical of LSDs, cells from MLIV patients contain large vesicles and accumulate lysosomal storage components (Bach, 2005). Nevertheless, the underlying bases of the MLIV symptoms are not known and there is no effective treatment.

A key advance was the discovery that MLIV results from loss-of-function mutations in TRP mucolipin 1 (TRPML1) (Bargal et al., 2000; Bassi et al., 2000; Sun et al., 2000). TRPML1 appears to be widely expressed and, consistent with the nature of MLIV, TRPML1 localizes to late endosomes and lysosomes (Manzoni et al., 2004). A *Caenorhabditis elegans* TRPML1 homolog, CUP-5, is also present in these organelles (Fares and Greenwald, 2001). Mutations in *cup-5* result in maternal-effect lethality, excessive cell death, and accumulation of large vacuoles (Hersh et al., 2002). However, a role for *cup-5* in the nervous system has not been described. Recently, a mouse MLIV model has been developed, which recapitulates many features of the disorder (Venugopal et al., 2007). Nevertheless, many critical questions remain regarding the cause of the progressive motor defects, neurodegeneration and the mechanistic link to lysosomal dysfunction. Most importantly, no concept has emerged that offers potential for developing therapies for treating MLIV.

Here, we report the development of *Drosophila* as an animal model for MLIV. We found that *trpml* mutant flies exhibited a phenotype remarkably reminiscent of MLIV. Most importantly, we report insights into the cellular mechanism underlying the neurodegeneration and motor impairments. Our findings provide a conceptual framework for developing strategies for treating this neurodegenerative disease.

RESULTS

Generation of Mutations in *Drosophila trpml*

The *Drosophila* genome encodes one TRPML homolog (CG8743), which shares ~40% amino acid identities with human TRPML1-3 (Figure 1A). Human *TRPML1* RNA is broadly expressed (Bargal et al., 2000; Bassi et al., 2000; Sun et al., 2000) and based on microarray studies, the fly *TRPML* RNA is also widely expressed, but at low levels (http://flyatlas.org/atlas.cgi?name=FBgn0036904). When expressed in HEK293 cells, yellow fluorescent protein (YFP)-tagged TRPML localized to lysosomes that were labeled by the low pH-specific dye, LysoTracker (Figure S1). Like human TRPML1 (Venkatachalam et al., 2006),

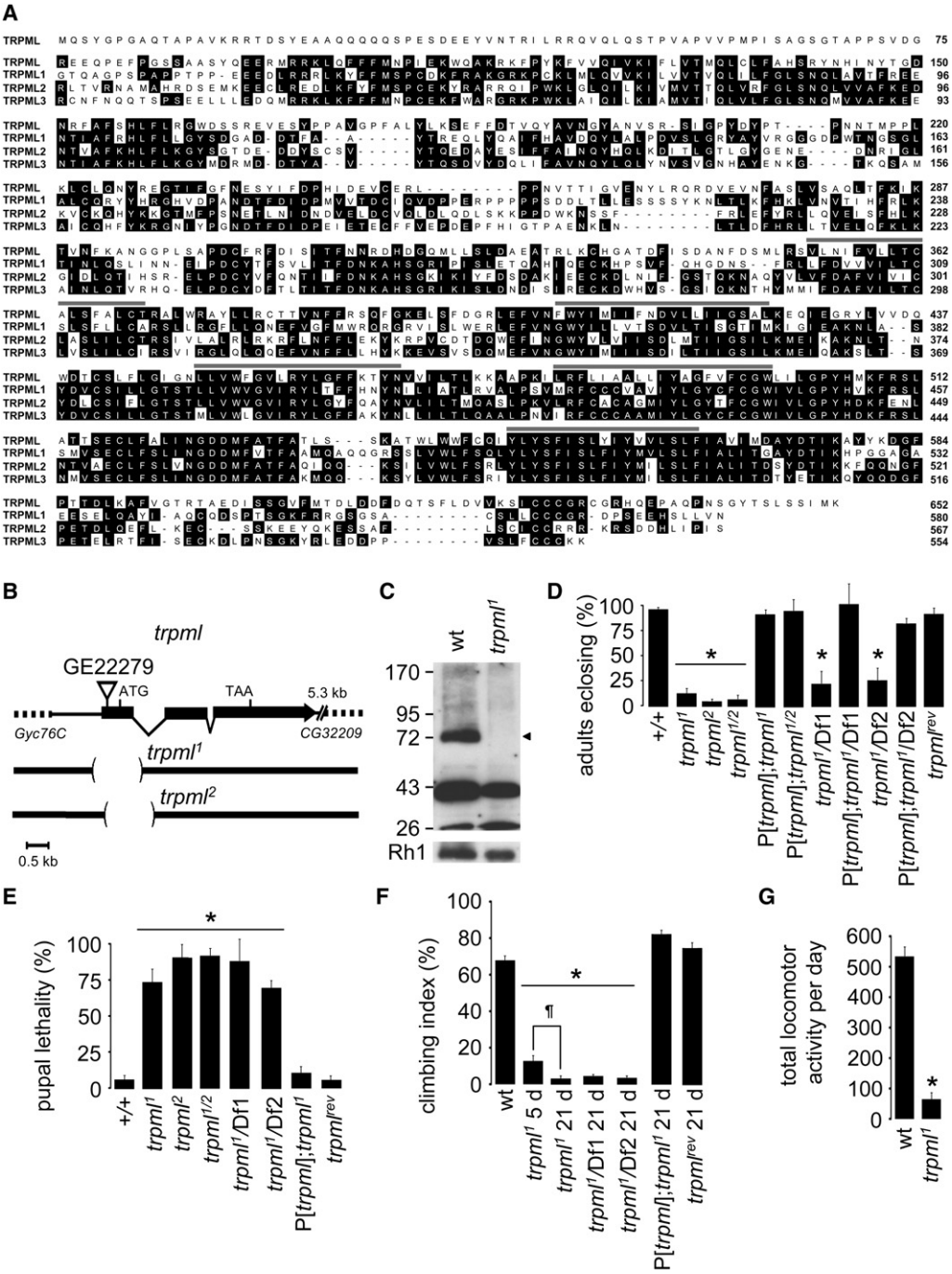

Figure 1. TRPML Is Required for Normal Viability and Motor Activity

(A) Alignment of *Drosophila* and human TRPML proteins. Lines indicate transmembrane domains.

(B) *trpml* genomic locus. The deletions in $trpml^1$ and $trpml^2$ are shown.

(C) Western blot of extracts from wild-type (WT) and $trpml^1$ flies probed with anti-TRPML antibodies and reprobed with anti-Rh1 antibodies (see Supplemental Experimental Procedures). The ~75 kDa band (arrowhead) corresponds to TRPML. The lower bands were due to nonspecific interactions with anti-TRPML.

(D) Percentage of pharate adults without the TM3 balancer after inter se crosses ($n \geq 4$ vials of each genotype; $^*p \leq 5 \times 10^{-6}$, ANOVA). Df1, *Df(3L)ED228*; Df2, *Df(3L)Exel6135*; P[*trpml*], genomic rescue; $trpml^{1/2}$, $trpml^1/trpml^2$; $trpml^{rev}$, precise excision.

(E) Percentage of dead pupae ($n = 4$ vials; $^*p \leq 0.005$, ANOVA).

(F) Climbing indices. Percentages of flies in a 50 ml glass cylinder that climb to the 25 ml mark in 15 s after being tapped down ($n \geq 13$, 10–20 flies each; $^*p \leq 5 \times 10^{-12}$, ANOVA; $^¶ p \leq 5 \times 10^{-4}$, t test).

(G) Number of crossings of an infrared beam (24 hr period) in an actometer ($n = 3$, 13–14 individual 5-day-old flies each; $^*p \leq 5 \times 10^{-11}$, t test).

Error bars represent SEM.

TRPML-YFP decorates the periphery of the lysosomes (Figure S1), indicating that it is a lysosomal membrane protein.

To generate a mutation in *trpml*, we obtained flies with a *P* element insertion (GE22279), 242 bases 5′ of the translation initiation site (Figure 1B). GE22279 flies had no obvious phenotype. We mobilized the transposon and identified two imprecise excision lines, with distinct 1.1 kb deletions, extending past the region encoding the first transmembrane domain (Figure 1B): $trpml^1$ and $trpml^2$ (−456 to +641 and −234 to +860 base pairs relative to the translation start site, respectively). We raised antibodies to TRPML, which were ineffective for immunostaining, but on Western blots recognized the predicted 75 kDa protein in wild-type fly extracts (∼75 kDa), which was undetectable in $trpml^1$ (Figure 1C).

Reduced Viability and Locomotor Activity in the *trpml* Mutants

To assess whether *trpml* was required for viability, we placed the mutations *in trans* with a balancer chromosome and performed inter se crosses. The percentages of viable adults without the balancer were significantly lower than in wild-type (Figure 1D; expected maximum of 33.3% scaled to 100%). When we placed $trpml^1$ *in trans* with $trpml^2$ ($trpml^{1/2}$) or either of two deficiencies spanning the *trpml* locus (76C3), the percentages of adults were similar to those obtained with the homozygous mutants (Figure 1D). The reduced viability was rescued by a wild-type *trpml* transgene (P[*trpml*]) and a line with a precise excision of the *P* element ($trpml^{rev}$) showed wild-type viability (Figure 1D). The reduced viability was due to pupal semilethality, since the percentage of dead pupae rose from <7% in wild-type, to >70% in the different *trpml* mutant combinations (Figure 1E).

A primary clinical manifestation of MLIV is a progressive deficit in motor function. To assess whether there was impaired motor function in the *trpml* mutants, we assayed negative geotaxis. After a tap to the bottom of a cylinder, 69.6% ± 3.0% of 5-day-old wild-type flies climbed to the top half within 15 s (Figure 1F). By 21 days, there was only a modest decrement in this activity (59.4% ± 3.5%). In contrast, only 12% ± 3.2% of 5-day-old $trpml^1$ flies ascended to the top half, and by 21 days the negative geotaxis was nearly eliminated (Figure 1F; 2.4% ± 1.2%), demonstrating a progressive loss of motor function. 21-day-old $trpml^1$ *in trans* with either deficiency displayed similarly reduced climbing, and the defect was rescued by the wild-type transgene (Figure 1F). We also assayed motor activity by placing 5-day-old flies in tubes for 24 hr, and tabulated the number of times they crossed an infrared beam. In this assay, $trpml^1$ flies also showed a significant reduction in activity (Figure 1G).

Progressive Neurodegeneration in the *trpml* Mutants

MLIV causes progressive neurodegeneration, including retinal degeneration. The fly compound eye consists of ∼800 ommatidia, each of which includes seven photoreceptor cells in each plane of section. Photoreceptor cells include a microvillar compartment, the rhabdomere, which is the site of phototransduction (Wang and Montell, 2007). In contrast to wild-type ommatidia, all of which had a full set of photoreceptor cells regardless of age, a significantly lower fraction of the ommatidia in 21-day-old $trpml^1$ flies retained all seven rhabdomeres (Figures 2A–2C; wild-type, 100%; $trpml^1$, 53.8% ± 9.9%; $p \leq 0.005$). This cell death was activity-dependent as 21-day-old dark-reared $trpml^1$ had a significantly higher fraction of ommatidia with all seven rhabdomeres (Figure 2C; 84.5% ± 4.8%; $p \leq 0.01$). This phenotype was progressive as all ommatidia in newly eclosed $trpml^1$ contained the full set of rhabdomeres (Figure 2C).

To determine whether there was progressive degeneration in *trpml* brains, we performed TUNEL staining. Old wild-type or young $trpml^1$ brains showed only minimal TUNEL staining (Figures 2D and S2A). In contrast, 21-day-old $trpml^1$ brains displayed increased TUNEL staining (Figures 2D–2F and S2E; arbitrary units: wild-type, 5.7 ± 0.7; $trpml^1$, 25.3 ± 1.2), which was rescued by the wild-type transgene (Figures S2C, S2D, and S2F). To identify the cell types that were dying, we costained 21-day-old $trpml^1$ and $trpml^1$/Df brains with TUNEL and antibodies that label the nuclei of neurons (αELAV) and glia (αREPO). Both neurons (Figures 2J–2L and S3D–S3F) and glia (Figures 2M–2O and S3F–S3I) were TUNEL positive.

Drosophila mutants displaying degeneration in the brain typically accumulate large vacuoles (Kretzschmar et al., 1997). The 21-day-old $trpml^1$ brains also showed a 4-fold increase in vacuoles (Figures S4A–S4C; wild-type, 1.8 ± 0.6; $trpml^1$, 7.4 ± 1.3). However, the vacuoles did not progress to the massive holes typical of other neurodegeneration mutants, potentially due to a defect in clearance of dead cells (see below).

Apoptotic cells have elevated phosphatidylserine (PS) in the outer plasma membrane leaflet due to increased translocation of PS from the inner leaflet during early apoptosis. Annexin A5 binds PS, providing a specific marker for apoptotic cells (van den Eijnde et al., 1998). Wild-type brains showed no annexin V-FITC staining. In contrast, 21-day-old $trpml^1$ brains displayed 10-fold elevated annexin V-FITC labeling (Figures 2P–2S and S5; wild-type, 3.4% ± 1.8%; $trpml^1$, 35.1% ± 10.9%; $p \leq 0.05$).

Increased Lysosomal Storage and Lipofuscin in *trpml* Mutant Flies

Many cell types in MLIV patients accumulate lysosome-like vesicles and autofluorescence (Goldin et al., 1995). Therefore, we evaluated whether *trpml* mutants displayed these features. All *trpml* mutant tissues examined had significantly elevated autofluorescence at 488 nm, including hemocytes (Figures S6A and S6D; arbitrary units: wild-type, 5.5 ± 0.5; $trpml^1$, 13.8 ± 1.7; $p \leq 0.01$), photoreceptor cells (Figures S6G and S6J; 14-day-old: wild-type, 2.4 ± 0.3; $trpml^1$, 9.3 ± 1.1; $p \leq 0.001$), and brains (Figures S6M and S6N; wild-type, 19.6 ± 0.6; $trpml^1$, 47.8 ± 4.8; $p \leq 0.005$). The autofluorescence was progressive, with a pronounced increase in *trpml* ommatidia and brains between Days 1 and 14 (Figures S7A and S7B; arbitrary units, $trpml^1$ brains: 1 day, 20.2 ± 0.8; 14 days, 47.8 ± 4.8; $p \leq 0.005$).

To determine whether the autofluorescence in $trpml^1$ cells was within lysosomes, we stained hemocytes and photoreceptor cells with LysoTracker and examined the staining at a wavelength (568 nm) at which autofluorescence was not detected. The autofluorescence colocalized with LysoTracker in hemocytes (Figures S6A–S6F) and photoreceptor cells (Figures S6G–S6L). The numbers of lysosomes also increased in the *trpml* mutants (Figures S6A–S6L; lysosomes/ommatidia: wild-type, 5.0 ± 0.8; $trpml^1$ 14.5 ± 2.1; $p \leq 0.0005$).

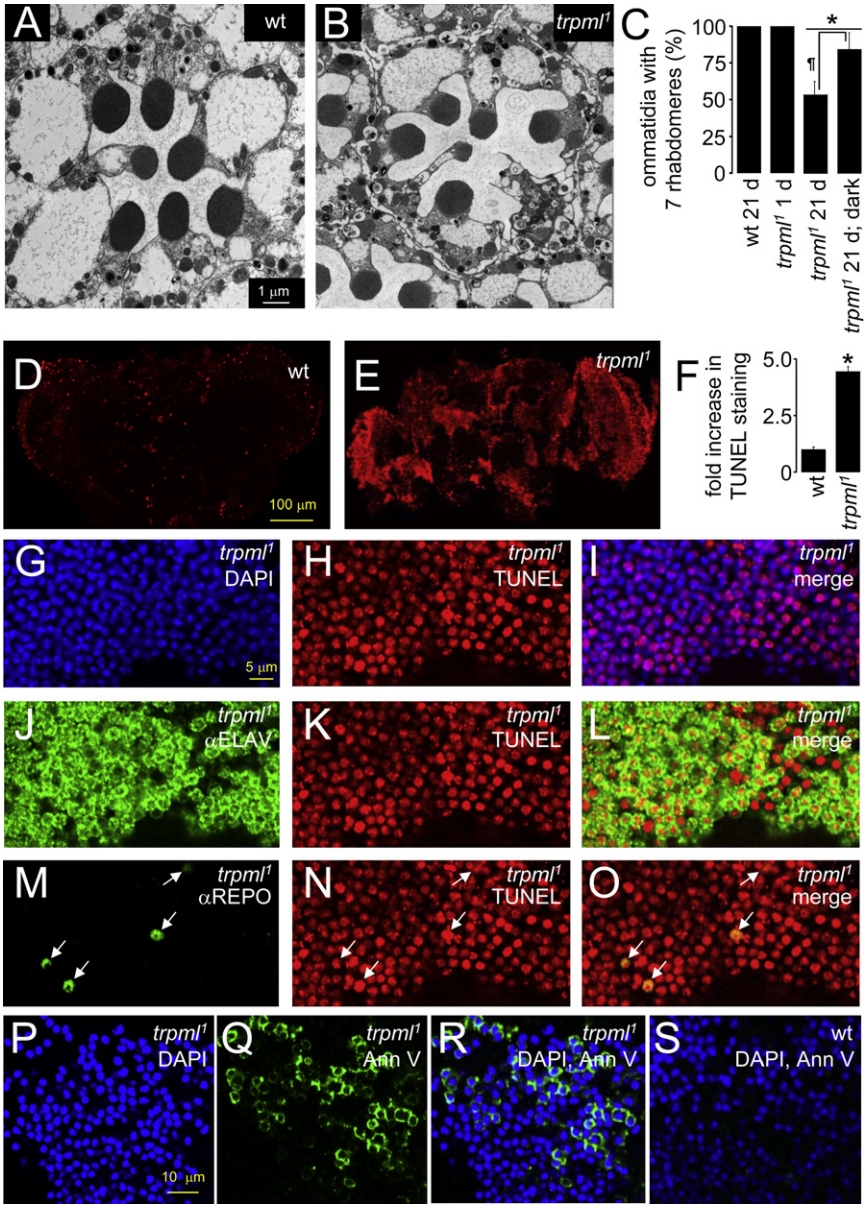

Figure 2. Neurodegeneration in *trpml* Retina and Brain

(A and B) Transmission EM of photoreceptor cells (21-day-old flies): (A) WT; (B) *trpml*^{1}.

(C) Percentages of ommatidia with a full set of seven rhabdomeres ($n \geq 3$ animals, ≥ 30 ommatidia per animal; *difference from WT, $p \leq 0.01$, ANOVA; ¶$p \leq 0.05$, t test).

(D and E) Confocal images of TUNEL-labeled brains (21-day-old flies): (D) WT; (E) *trpml*^{1}.

(F) Fold increase in TUNEL labeling in *trpml*^{1} normalized to WT mean ($n = 3$; *$p \leq 5 \times 10^{-4}$, t test).

(G–I) Confocal images of brains from 21-day-old *trpml*^{1} viewed at 310 nm to detect DAPI (G) and 568 nm to detect TUNEL (H). (I) Merged image.

(J–L) Same as (G–I), but brains viewed at 633 nm to detect ELAV (J).

(M–O) Same as (G–I) but brains viewed at 488 nm to detect REPO (M). Arrows indicate glia.

(P–R) Confocal images of 21-day-old *trpml*^{1} brains viewed at 310 nm to detect DAPI (P) and 488 nm to detect annexin V-FITC (Q). (R) Merged image.

(S) Same as (R), but with 21-day-old WT brains.

Error bars represent SEM.

Lysosomal autofluorescence is indicative of lipofuscin (polymerized nondegradable protein and lipid-containing material in the lysosomal lumen; Terman and Brunk, 2004). To address whether the autofluorescence in *trpml* cells was from lipofuscin, we examined the spectral properties of extracted lipids. The peaks characteristic of lipofuscin are distinct from other types of autofluorescence, such as porphyrins. In *trpml*^{1}, the excitation and emission maxima matched lipofuscin (Figure S6O; ~380 and 460 nm) (Fletcher et al., 1973).

Defective Autophagy and Mitochondrial Dysfunction in *trpml* Neurons

Lipofuscin accumulation indicates disrupted autophagy, a lysosomal degradation process impaired in many neurodegenerative diseases (Klionsky, 2007). Defective autophagy can lead to either an accumulation of autophagosomes, which contain components that are normally degraded after these vesicles fuse with lysosomes, or an accumulation of autolysosomes if fusion with lysosomes proceeds normally but lysosomal proteolysis is disrupted (Klionsky, 2007). To determine whether *trpml* cells amassed autophagosome-like vesicles, we performed transmission electron microscopy (EM) on retinal sections. In photoreceptor cell bodies from 21-day-old *trpml*^{1}, there were 6.5-fold more cytoplasmic membrane inclusions than in wild-type (Figures 3A–3E; vesicles/cell body: wild-type, 0.85 ± 0.2; *trpml*^{1}, 5.6 ± 0.9). These membranous inclusions varied in diameter (0.2–1.0 μm), and consisted of multilamellar and multivesicular bodies (Figure 3D). The multilamellar vesicles displayed the morphological hallmarks of autophagosomes—membranous compartments containing internal membranous structures and cytoplasmic material (Mizushima, 2004). The multivesicular bodies may be late endosomes (Dermaut et al., 2005). The accumulation of the cytoplasmic membrane inclusions *trpml*^{1} was age dependent (vesicles/cell body: 1-day-old, 0.5 ± 0.2; 21-day-old, 5.6 ± 0.9; $p \leq 0.0001$).

To assay further whether there was an increase in autophagosomes in *trpml*^{1}, we used an autophagosomal marker, GFP-ATG8 (Scott et al., 2004) and performed imaging under conditions in which autofluorescence had dissipated. The 21-day-old *trpml*^{1} brains showed double the GFP-ATG8 fluorescence compared with wild-type (Figures 3F–3H; 1.96 ± 0.1-fold elevation), while the number of GFP-ATG8-positive vesicles in 21-day-old

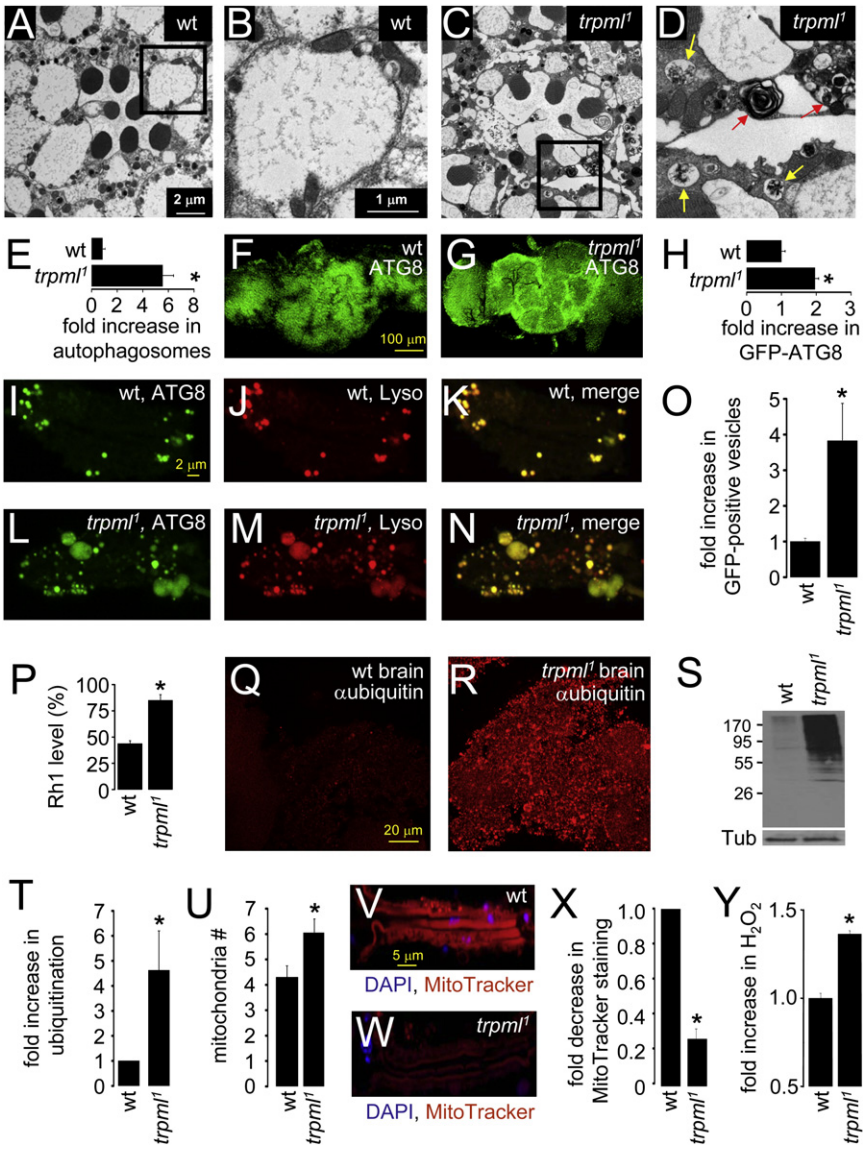

Figure 3. Disruption of Autophagy in Neural Tissues in *trpml*

(A–D) Transmission EM of 21-day-old photoreceptor cells: (A and B) WT; (C and D) *trpml*^{1}. (B and D) Magnifications of the boxed regions in (A and C). The red and yellow arrows in (D) indicate multilamellar and multivesicular bodies respectively.

(E) Fold increase in autophagosome-like vesicles in *trpml*^{1} photoreceptors (n = 5 animals, ≥30 ommatidia per animal; *$p \leq 10^{-4}$).

(F and G) Brains (21-day-old flies) expressing GFP-ATG8 and viewed at 488 nm: (F) WT; (G) *trpml*^{1}.

(H) Fold increase in GFP-ATG8 fluorescence in *trpml*^{1} brains (n = 3; *$p \leq 5 \times 10^{-4}$).

(I–N) Ommatidia from 21-day-old flies expressing GFP-ATG8: (I–K) control; (L–N) *trpml*^{1}. Ommatidia were viewed at 488 nm to detect GFP-ATG8 (I–L) and 568 nm to detect LysoTracker (Lyso; J–M). (K and N) Merged images.

(O) Fold increase in GFP-positive vesicles in *trpml*^{1} ommatidia (n = 3 independent experiments; *$p \leq 5 \times 10^{-5}$).

(P) Rh1 remaining after 6 hr exposure to blue light (480 nm) in 5-day-old flies. Means are relative to the starting value (defined as 100%) (n = 3; *$p \leq 0.05$).

(Q and R) Four wk-old brains stained with anti-ubiquitin antibodies (Supplemental Experimental Procedures): (Q) WT; (R) *trpml*^{1}.

(S) Western blot of head extracts (4 wk-old flies) probed with anti-ubiquitin antibodies and re-probed with anti-tubulin antibodies.

(T) Fold increase of ubiquitination in head extracts based on Western blotting. Data were normalized to WT (1.0) (n = 3; *$p \leq 0.05$).

(U) Mitochondria per photoreceptor cell in 21-day-old WT flies (n = 5 animals; *$p \leq 0.05$).

(V and W) Ommatidia from 21-day-old WT (V) and *trpml*^{1} (W) flies viewed at 310 nm to detect DAPI (blue) and 568 nm to detect MitoTracker-orange CM-H2TMRos (red).

(X) Fold decrease in MitoTracker-orange CM-H2TMRos staining in *trpml*^{1} head extracts, normalized to WT (set at 1.0) (n = 3; *$p \leq 5 \times 10^{-6}$).

(Y) Relative H_2O_2 levels in whole fly extracts. Data were normalized to WT (set at 1.0) ($n \geq 6$, 10 flies/experiment; *$p \leq 5 \times 10^{-6}$). Dissected brains and ommatidia were viewed by confocal microscopy. All statistical data are the result of t tests; error bars represent SEM.

mutant ommatidia increased nearly 4-fold (Figures 3I–3O; 3.8 ± 1.0).

In some LSDs, the buildup of autophagosomes results from a disruption in fusion of autophagosomes with lysosomes (Settembre et al., 2007). To address whether there was a defect in fusion in *trpml*^{1}, we tested for colocalization of markers for autophagosomes (GFP-ATG8) and lysosomes (LysoTracker). In contrast to other LSDs, the autophagosome and lysosome markers overlapped (Figures 3I–3N; wild-type, 91% ± 4.6%; *trpml*^{1}, 89% ± 2.9%). Thus, it appeared that there was no reduction in autophagosome-lysosome fusion. Rather, *trpml*^{1} neurons accumulated autolysosomes, consistent with a defect in proteolytic degradation following fusion of lysosomes and autophagosomes.

To test for a defect in lysosomal degradation, we evaluated whether blue light (480 nm)-induced degradation of rhodopsin1 (Rh1) was reduced in *trpml*^{1} photoreceptor cells, since blue light exposure leads to constitutive activation of Rh1, endocytosis, and degradation in lysosomes (Xu et al., 2004). A 6 hr exposure to blue light caused an ~55% reduction of Rh1 levels in wild-type, while *trpml*^{1} showed only an ~15% decrease (Figure 3P; Rh1 remaining: wild-type, 43.8% ± 0.1%; *trpml*^{1}, 85% ± 0.1%; $p \leq 0.05$).

Mammalian TRPML1 has been reported to be a proton-permeable channel, providing a proton leak pathway in the lysosomal membrane (Soyombo et al., 2006). Therefore, loss of TRPML1 leads to over-acidification of the lysosomal lumen in tissue

culture cells (Miedel et al., 2008). As an indirect measure of intralysosomal pH, we relied on the intensities of LysoTracker staining and found that lysosomes of relatively the same size were significantly brighter in *trpml*^{1} photoreceptor cells (Figure S8, arbitrary units: wild-type, 17.3 ± 2.0; *trpml*^{1}, 46 ± 3.5; $p \leq 10^{-5}$). This result may indicate over-acidification of lysosomes in the *trpml* mutant.

Autophagic and proteosomal pathways are coupled such that incomplete autophagy can cause macromolecules that are normally degraded by autophagy to enter the proteosomal pathway, thereby increasing the levels of polyubiquitinated proteins (Settembre et al., 2007). We found that *trpml*^{1} brains (Figures 3Q and 3R) and head extracts showed significantly elevated antiubiquitin staining (Figures 3S and 3T; 4.6 ± 1.6-fold higher).

Inhibition of autophagy can lead to the accumulation of damaged mitochondria and oxidative stress (Terman and Brunk, 2004). Mitochondria undergo cycles of fusion and fission, which sometimes gives rise to uneven daughters, one of which has a disrupted transmembrane potential ($\Delta\Psi$) and is targeted for degradation via autophagy (Twig et al., 2008). Therefore, disruption of autophagy can lead to accumulation of damaged mitochondria. We found that photoreceptor cell bodies from 21-day-old *trpml*^{1} displayed a small but significant increase in the number of mitochondria (Figure 3U; wild-type, 4.3 ± 0.4; *trpml*^{1}, 6.0 ± 0.5; $p \leq 0.05$). Although the number of mitochondria increased, the intensity of Mitotracker-orange CM-H2TMRos staining in *trpml*^{1} ommatidia was reduced 4-fold relative to wild-type (Figures 3V–3X; arbitrary fluorescence units: wild-type, 29 ± 1.8; *trpml*^{1}, 7.8 ± 1.0; $p \leq 5 \times 10^{-6}$). Since mitochondrial uptake of Mitotracker-orange CM-H2TMRos is dependent upon functional $\Delta\Psi$ (Deshmukh et al., 2000), the accumulation of mitochondria with dissipated $\Delta\Psi$ in *trpml*^{1} neurons is indicative of a disruption of autophagic clearance of dysfunctional mitochondria.

One indication of oxidative stress in *trpml*^{1} was the increase in lipofuscin. To evaluate oxidative stress in *trpml*^{1} further, we measured the levels of the reactive oxygen species, H_2O_2, and found that the mutant flies showed ~40% higher H_2O_2 levels compared with controls (Figure 3Y; $p \leq 5 \times 10^{-6}$). This elevation is physiologically significant, since 30%–60% increases in H_2O_2 can induce abnormally high apoptosis and neurodegeneration (Li et al., 2000; St.-Pierre et al., 2006).

Loss of *trpml* Enhances Polyglutamine-Mediated Neurotoxicity

Introduction of a polyglutamine repeat in the *Drosophila* eye results in macromolecular aggregation and cytotoxicity (Warrick et al., 1999). Upregulation of autophagy promotes the clearance of these aggregates, thereby suppressing polyglutamine-mediated toxicity (Ravikumar et al., 2004). To test whether defective autophagy in *trpml*^{1} enhanced polyglutamine-mediated toxicity, we expressed a 120 polyglutamine repeat protein in *trpml*^{1} photoreceptor cells (*gmr-HDQ120*) (Warrick et al., 1999) and used an assay on intact eyes to test for loss of rhabdomeres (Figure 4A). Most newly eclosed *trpml*$^+$ flies expressing *gmr-HDQ120*/+ had a full set of seven rhabdomeres, but displayed rapid retinal degeneration during the first 3 days posteclosion (Figures 4A and 4B). In combination with the *trpml*^{1} mutation, the time course of degeneration was enhanced significantly, starting from the day of eclosion (Figures 4A and 4B). In the absence of *gmr-HDQ120*, the *trpml*^{1} mutation did not cause rhabdomere loss over this time span (Figure 4B). Since autophagy protects against polyglutamine-induced toxicity, the result that *trpml*^{1} enhances *HDQ120*-mediated neurotoxicity is consistent with disrupted autophagy in *trpml*^{1} neurons.

Targeted Expression of *hspA1L* in Neurons Restores Viability and Motor Function

A factor contributing to the cell death from protein aggregation is the irreversible association of molecular chaperones with these aggregates, thereby lowering the level of chaperones available for newly synthesized proteins (Brignull et al., 2007). Increasing expression of the molecular chaperone Heat Shock Protein 70 (HSP70), or introduction of the human homolog, HSPA1L, protects against polyglutamine repeat neuronal toxicity in the *Drosophila* eye (Warrick et al., 1999).

We assessed the effectiveness of suppressing the pupal semilethality and motor deficits in *trpml*^{1} by introduction of *hspA1L*. Expression of *UAS-hspA1L* using either ubiquitous or neuronal *GAL4* drivers rescued the pupal semilethality (Figure 4C), while expression in glia and fat bodies/hemocytes did not (Figure 4C). Introduction of *hspA1L* in neurons also restored normal motor activity in *trpml*^{1} flies (Figure 4D). Thus, it appeared that the primary defect leading to the increased lethality and motor deficits in *trpml*^{1} animals occurred in neurons. The rescue of the locomotor activity may be attributed to a suppression of the elevated cell death. Therefore, we assayed annexin V-FITC labeling in *hspA1L*-expressing neurons and found significant rescue of the cell death (Figures 4E and 4F; annexin V-labeled cells: wild-type, 3.4% ± 1.8%; *trpml*^{1}, 35.1% ± 10.9%; *hspA1L* and *trpml*^{1}, 10.7% ± 3.0%, not significantly different from wild-type).

Disruption of Synaptic Transmission in the Absence of TRPML

We noticed that the *trpml*^{1} flies remained immobilized longer than wild-type after exposure to CO_2 anesthesia. After 4 min, 90.7% ± 9.3% of wild-type recovered mobility, in contrast to only 6.7% ± 3.3% of *trpml*^{1}. The return of activity of all *trpml*^{1} flies required 9 min—twice as long as for wild-type (Figure 5A). Since CO_2 immobilizes flies through inhibition of synaptic transmission at the neuromuscular junction (NMJ) (Badre et al., 2005), we tested whether there was a decrease in synaptic transmission in *trpml*^{1}. This possibility seemed plausible given that increased oxidative stress correlates with reduced NMJ synaptic transmission (Giniatullin et al., 2006).

To assess synaptic function, we made evoked excitatory junction current (EJC) recordings at the NMJ synapse of 3rd instar larvae, using the two-electrode voltage-clamp (TEVC) configuration. To reveal changes in basal synaptic function, we performed assays in a bath solution containing 0.5 mM extracellular [Ca^{2+}] (Rohrbough et al., 1999; Trotta et al., 2004). Control animals exhibited a mean EJC amplitude of 64.1 ± 5.2 nA, while *trpml*^{1} showed an ~50% decrease in transmission strength (32.3 ± 4.6 nA; Figures 5B and 5C).

To investigate whether the reduction in synaptic transmission was due to an alteration in the size or cycling of the endo-exo synaptic vesicle (SV) pool, we used the lipophilic fluorescent dye FM1-43 to assay SV endocytosis and exocytosis (Kuromi

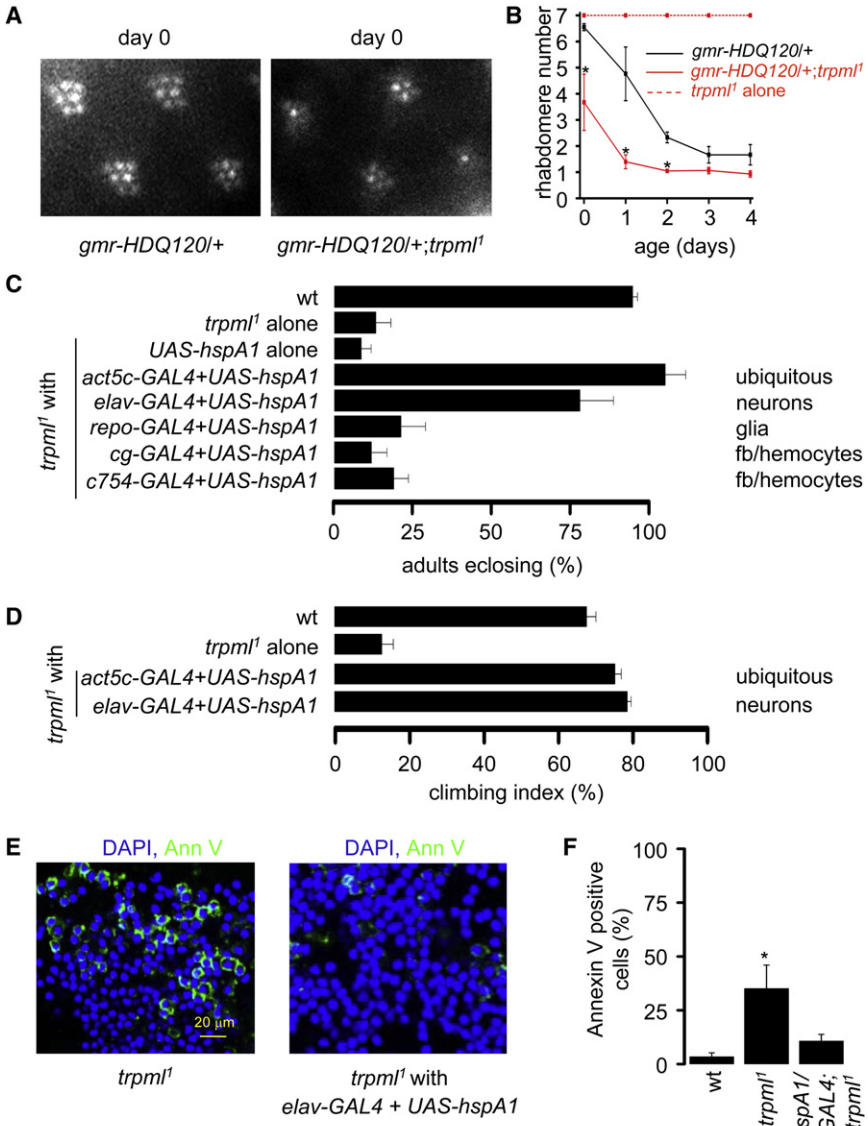

Figure 4. Toxic Aggregation of Macromolecules in *trpml*

(A) Ommatidia viewed by the optical neutralization technique ≤24 hr posteclosion.

(B) Time course of photoreceptor degeneration viewed by optical neutralization (n ≥ 3 flies, ≥50 ommatidia/fly; *difference at each time point, $p \leq 0.05$).

(C) Percentage of pharate adults without the TM3 balancer in WT, *trpml*^{1}, and *trpml*^{1}, with the indicated transgenes (n = 7–11). GAL4 expression is indicated; fb, fat bodies.

(D) Climbing indices (n = 3–8, 10–20 flies each).

(E) Merged confocal images of brains from 21-day-old flies viewed at 310 nm to detect DAPI and 488 nm to detect annexin V-FITC.

(F) Percentages of adult brain cells labeled with annexin V-FITC (n ≥ 3 brains; *difference from WT, $p \leq 0.05$).

All statistical data are the result of t tests; error bars represent SEM.

and Kidokoro, 2000; Fergestad and Broadie, 2001; Trotta et al., 2004). We exposed NMJ preparations to FM1-43 in the presence of 90 mM [K$^+$] saline, which depolarized the nerve terminal and induced vesicular cycling and loading of FM1-43. We then depolarized the preparations in the absence of FM1-43 to assess dye unloading by SV exocytosis. Based on comparison of the initial mean fluorescence values, *trpml* mutant synaptic boutons displayed a 4-fold decrease in loading (Figures 5D and 5E; wild-type, 187.3 ± 9.3; *trpml*^{1}, 48.2 ± 3.2). This lower level of loading was sufficient to assess whether the loaded boutons in *trpml*^{1} unloaded properly. Following the second depolarization, the wild-type boutons displayed a >90% reduction in fluorescence (unloading), whereas the *trpml*^{1} mutants showed little decrease (Figures 5D and 5E; wild-type, 29.2 ± 3.5; *trpml*^{1}, 39.3 ± 3.6). These data indicate that the diminished synaptic transmission in *trpml*^{1} was due to presynaptic impairment of SV cycling.

Expression of *trpml*$^+$ in Neurons, Hemocytes, or Glia Rescues *trpml* Phenotypes

To determine the cellular requirements for TRPML, we expressed wild-type *UAS-trpml* under the control of *promoter-GAL4* transgenes that were expressed in different cell types. Introduction of the *UAS-trpml* transgene alone in *trpml*^{1} had no impact on pupal semilethality, the behavioral climbing index, or synaptic transmission amplitude. However, these deficits were rescued fully upon expression of *UAS-trpml* under the control of ubiquitously expressed (*act5c-GAL4*) or panneuronally expressed (*elav-GAL4*) *GAL4* drivers (Figures 6A–6D).

As controls, we expressed *UAS-trpml* using *GAL4*s that directed expression in follicle cells (*e22c-GAL4*), hemocytes/fat bodies (*cg-GAL4, c754-GAL4* and *hml-GAL4*), and glia (*repo-GAL4*). As expected, the combination of the *e22c-GAL4* with *UAS-trpml* did not improve adult viability (Figure 6A). To our surprise, the hemocyte/fat body and glial drivers restored normal survival, climbing activity, and synaptic transmission (Figures 6A–6D). While the onset of motor deficits following the expression of *trpml*$^+$ in glia or hemocytes/fat bodies was delayed significantly, there was some subsequent age-dependent decline in climbing activity (Figure 6E). Nevertheless, the significant rescue of the *trpml*^{1} impairments by expression in hemocytes/fat bodies or glia was unanticipated, since we expected that the *trpml*^{1} phenotypes were due to loss of function solely in neurons.

Accumulation of Late-Apoptotic Cells Suppressed by Expression of *trpml*$^+$ in Hematopoietic Cells

In *Drosophila*, both hemocytes and glia are involved in the clearance of apoptotic cells during development and in the adult

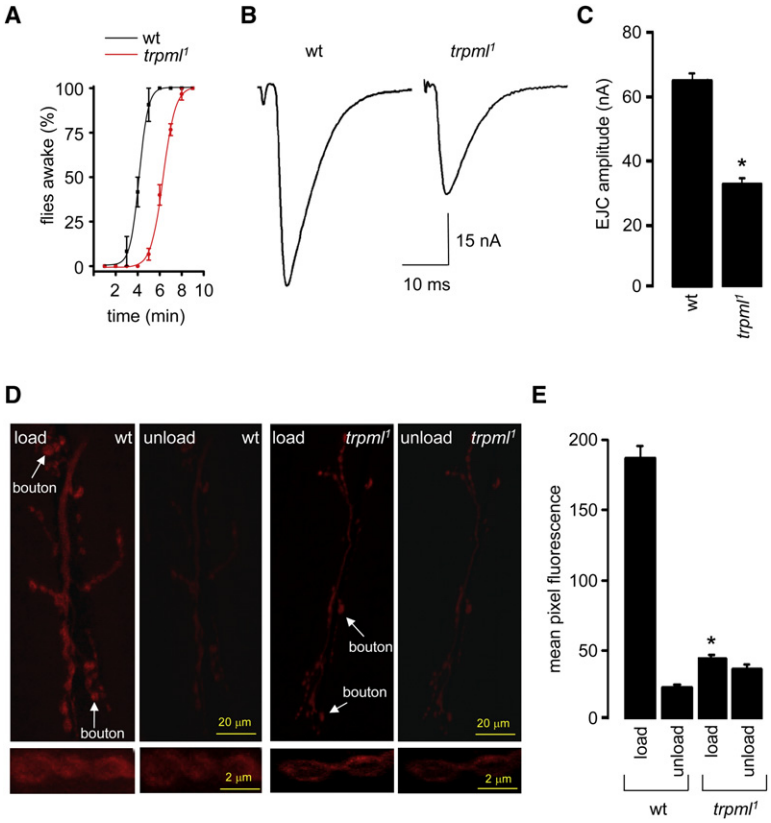

Figure 5. Impairment of Synaptic Transmission in the *trpml*

(A) Time course of flies with restored mobility following a 3 min exposure to CO_2 (n = 3, 10 flies per experiment).

(B) EJC from the third instar NMJ.

(C) Quantification of the EJC amplitudes in WT and *trpml*^{1} (n = 5 animals; 10 NMJs for each genotype; *$p \leq 0.001$).

(D) NMJ synapses following FM1-43 loading and unloading. Arrows indicate synaptic boutons. Panels below show enlarged magnification of synaptic boutons.

(E) Quantification of FM1-43 fluorescence intensity in NMJ boutons following dye loading and unloading. n = 5 animals,10 NMJs for each genotype; *, difference from WT, $p \leq 0.001$. All statistical data are the result of t tests; error bars represent SEM.

nervous system (Wood and Jacinto, 2007). Clearance of dead cells is particularly important during developmental stages in which there is pronounced apoptosis, such as during pupal-to-adult metamorphosis and late neural development, when many surplus cells are pruned (Lee and Baehrecke, 2001; Awasaki et al., 2006). Rapid clearance of early-apoptotic neurons minimizes neuroinflammation, which otherwise occurs through the release of antigenic material by late-apoptotic cells with compromised plasma membranes (Franc, 2002). Late-apoptotic and necrotic cells release cytotoxic agents, which can induce cell death in neighboring cells, thereby leading to widespread neurodegeneration. Several aspects of the *trpml*^{1} phenotype raised the possibility that there was a buildup of late-apoptotic and necrotic cells, indicative of a defect in clearance. These include widespread neurodegeneration and rescue of these phenotypes by reintroduction of *trpml*$^+$ in hemocytes and glia.

To address whether there was accumulation of late-apoptotic and necrotic cells in *trpml*^{1}, we stained brains with annexin V-FITC or propidium iodide (PI). PI is a membrane-impermeant nuclear dye that only stains cells that have lost plasma membrane integrity due to cell death (Franc et al., 1999). Annexin V-FITC staining without PI staining is indicative of early-apoptotic cells with an intact plasma membrane. Late-apoptotic/necrotic cells have compromised membrane integrity. Therefore, staining with both annexin V-FITC and PI is indicative of an accumulation of late-apoptotic/necrotic cells (Franc et al., 1999). We performed staining with annexin V-FITC on unfixed tissue, while we used fixed tissue for PI staining, since the duration of the procedure without fixation caused necrosis in intact adult brains, possibly due to acute hypoxia. The 21-day-old *trpml*^{1} brains showed significant increases in the percentage of cells with annexin V-FITC membrane staining (Figures 7A and 7B; wild-type, 3.4% ± 1.8%; *trpml*^{1}, 35.1% ± 10.9%; $p \leq 0.05$) and PI-positive nuclei (Figures 7A and 7B; wild-type, 0.1 ± 0.1%; *trpml*^{1}, 35.5% ± 11%; $p \leq 10^{-5}$). These data demonstrate that there was a significant elevation in the accumulation of late-apoptotic/necrotic cells in *trpml* brains, indicating a deficit in the clearance of dying cells.

To determine whether expression of *trpml* in hematopoietic and glial cells reduced the accumulation of late-apoptotic/necrotic cells, we expressed *UAS-trpml* under the control of the *GAL4* lines described above. Upon expression of *UAS-trpml* using the panneuronal *GAL4* (*elav-GAL4*), there was virtually no staining with annexin V-FITC or PI, similar to wild-type (Figures 7A and 7B). When we expressed *UAS-trpml* in hemocytes/fat bodies (*cg-GAL4*) or glia (*repo-GAL4*), the number of late-apoptotic cells again returned to the very low levels typical of wild-type, although early-apoptotic cells were still detected (Figures 7A and 7B). Since only panneuronal expression of *trpml* fully suppresses cell death, these results suggest that the initial cell death occurs in neurons and that *trpml* expression in hemocytes or glia contributes to clearance of dying neurons. Consistent with this observation, *trpml* expression in neurons abolished all cell death in the adult brain (Figure 7C). The glial cell death that occurred in *trpml*^{1} brains (Figures 2M–2O) was also rescued by expression of *trpml* in neurons (Figure 7C). Although we cannot exclude that *elav-GAL4* is expressed in some glia, our results indicate that glial cell death occurs in a non-cell-autonomous manner and is a secondary consequence of a defect in the clearance of adjoining apoptotic neurons. Since necrotic cells also display DNA fragmentation (Pang and Geddes, 1997), the increased TUNEL staining of neurons and glia in *trpml*^{1} brains could indicate pronounced secondary necrosis due a defect in the clearance of apoptotic neurons.

The *croquemort* (*crq*) gene encodes a CD36-related scavenger receptor, which is involved in the clearance of cells undergoing both apoptotic and autophagic cell death (Franc et al., 1999; Lee and Baehrecke, 2001). Although predominantly expressed

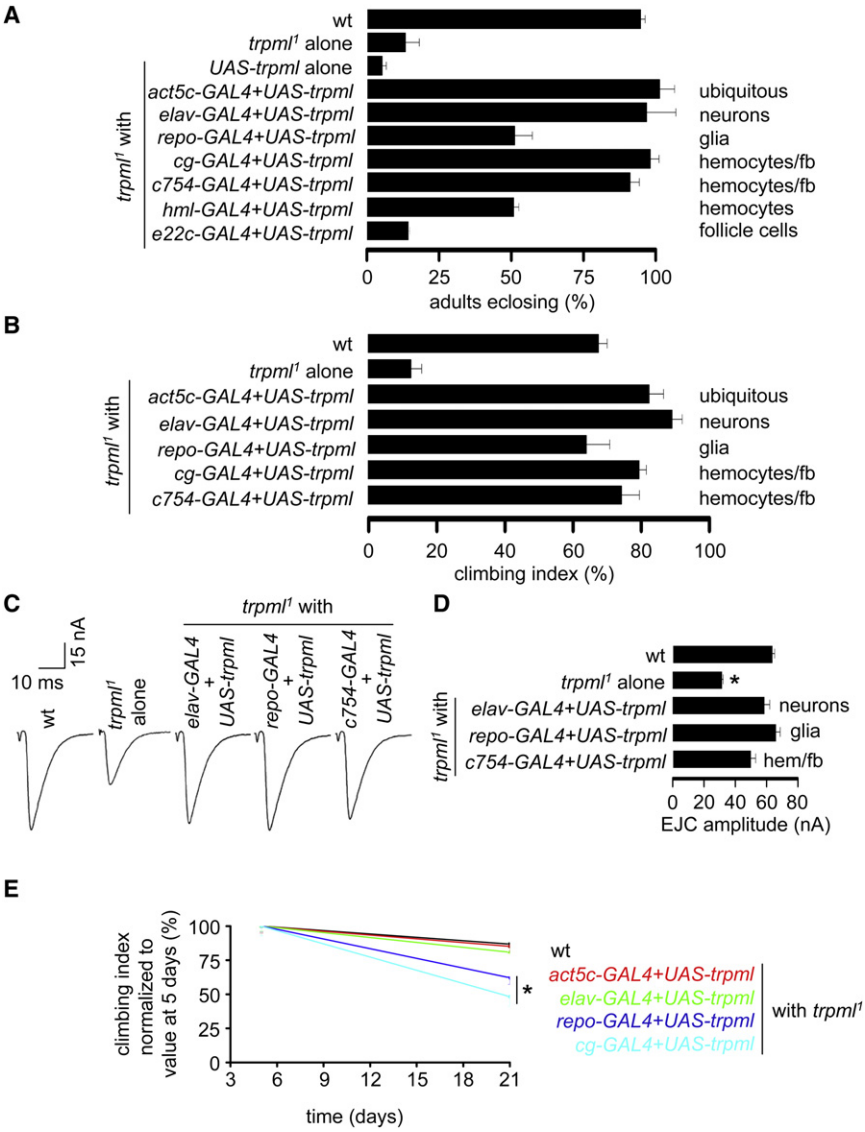

Figure 6. TRPML Expression in Either Hemocytes/Fat Bodies or Glia Rescues the *trpml* Pupal Semilethality, Locomotor Defects, and Synaptic Transmission Impairment

(A) Percentage of pharate adults without the TM3 balancer (n = 7–11). *GAL4* expression patterns are indicated.

(B) Climbing indices of adult flies (n = 3–8 experiments, 10–20 flies each).

(C) Representative EJC traces of larvae.

(D) Quantification of the EJC amplitudes (n = 5 animals, 10 NMJs for each genotype; *$p \leq 10^{-4}$, ANOVA). hem, hemocytes.

(E) Age-progressive decline in climbing index of WT (black) and *trpml*[1] flies expressing *UAS-trpml* and the indicated *GAL4*s. Indices are normalized with 5 day values as 100% ($n \geq 3$, 10–20 flies per experiment; *difference from WT, $p \leq 0.05$, ANOVA).

Error bars represent SEM.

in macrophage populations, exogenous expression of *crq* in COS cells confers on them the ability to phagocytize apoptotic cells (Franc et al., 1996). Therefore, we tested whether expression of *crq* in *trpml*[1] neurons enabled them to phagocytize nearby apoptotic cells, thereby preventing the accumulation of late-apoptotic/necrotic cells and the locomotor defects. Furthermore, since autophagic cell death promotes the removal of superfluous tissues during pupal metamorphosis (Franc et al., 1999; Lee and Baehrecke, 2001), the pupal semilethality in *trpml*[1] might also be due to a defect in autophagic cell clearance in the developing nervous system and be suppressed by increasing expression of *crq* in *trpml*[1] neurons.

To test whether exogenous overexpression of *crq* rescues the defects associated with *trpml*, we drove expression of *UAS-crq* using either panneuronal or hemocyte *GAL4*s (*elav-GAL4* or *hml-GAL4* respectively). Introduction of the *UAS-crq* transgene alone in *trpml*[1] had no impact, whereas expression of *crq* in neurons or hemocytes rescued the pupal semilethality (Figure 7D; $p \leq 0.05$). Furthermore, the motor defect was suppressed significantly in 5-day-old *trpml*[1] by neuronal expression of *crq* (Figure 7E; $p \leq 5 \times 10^{-5}$). Expression of *crq* in brain neurons also decreased TUNEL labeling, and the residual staining was only in neurons (Figure 7F). This further supports the finding that primary cell death occurs in neurons, and reduced clearance of apoptotic neurons induces secondary death in adjoining cells, including glia.

DISCUSSION

Requirement for TRPML for Lysosomal Function and Completion of Autophagy

Impairments in autophagy are implicated in the pathophysiology of several neurodegenerative diseases (Klionsky, 2007). MLIV may also involve a perturbation in autophagy, as suggested by a pharmacological study using a tissue culture model (Jennings et al., 2006). We found that *trpml* mutant cells displayed impaired autophagy in vivo. However, in contrast to other models of LSDs (Settembre et al., 2007), there does not appear to be a block in fusion between the lysosomes and autophagosomes in *trpml* cells. Rather, there appeared to be reduced macromolecular degradation in autolysosomes following fusion.

Recent in vitro studies suggest that mammalian TRPML1 is a proton-permeable channel that provides a proton leak pathway in the lysosomal membrane (Soyombo et al., 2006; Miedel et al., 2008). Therefore, in the absence of the channel, we propose that over-acidification of the lysosomal lumen impairs normal degradation in autolysosomes, since lysosomal proteases are intimately dependent on the normal lysosomal pH.

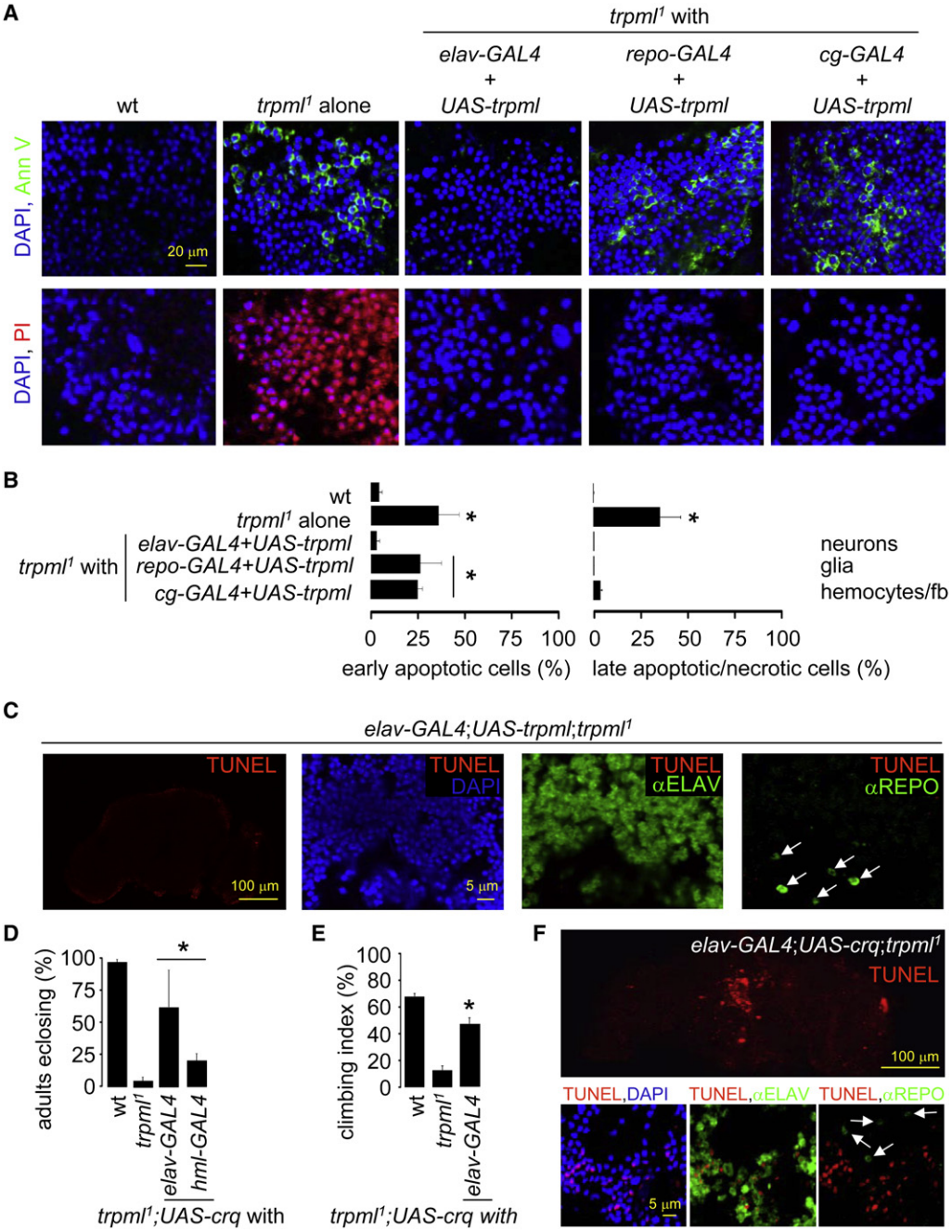

Figure 7. Reduced Clearance of Late-Apoptotic Cells in *trpml* Mutants

Images are by confocal microscopy.

(A) DAPI/annexin V-FITC- and DAPI/PI-stained brains from 21-day-old flies.

(B) Percentage of early-apoptotic and late-apoptotic/necrotic cells in brains from 21-day-old flies ($n \geq 3$; *difference from WT, $p \leq 0.01$, ANOVA).

(C) Brains from 21-day-old flies viewed at 310 nm to detect DAPI, 488 nm to detect anti-REPO, 568 nm to detect TUNEL, and 633 nm to detect anti-ELAV. Arrows indicate glia.

(D) Percentage of pharate adults without the TM3 balancer (n = 3–11; *difference from *trpml*^{1}, $p \leq 0.05$, ANOVA).

(E) Climbing indices of adult flies ($n \geq 5$; *difference from *trpml*^{1}, $p \leq 5 \times 10^{-5}$, t test).

(F) Brains from 21-day-old flies viewed at 310 nm to detect DAPI, 488 nm to detect anti-REPO, 568 nm to detect TUNEL, and 633 nm to detect ELAV. Arrows indicate glia.

Error bars represent SEM.

Mitochondrial Dysfunction and Oxidative Stress in *trpml* Mutant

In addition to playing a cytoprotective role by promoting clearance of toxic macromolecules, autophagy is important for the turnover of entire organelles, including damaged mitochondrial with disrupted $\Delta\Psi$ (Twig et al., 2008); *trpml* neurons accumulated mitochondria with dissipated $\Delta\Psi$, indicating disruption of autophagic clearance of dysfunctional mitochondria. Moreover, *trpml* cells accumulated lipofuscin, indicative of oxidative stress, and the mutant animals displayed a significant increase in H_2O_2 in a range that leads to elevated apoptosis and neurodegeneration (Li et al., 2000; St.-Pierre et al., 2006). Thus, oxidative stress appears to be a key factor contributing to the neurodegeneration in the *trpml* mutant.

The Molecular Chaperone, HSP70, Suppresses the *trpml* Phenotype

To cope with oxidative stress and toxic aggregation of macromolecules, cells increase expression of molecular chaperones, such as hsps (Ménoret et al., 2002). Exogenous expression of the human homolog of HSP70 (HSPA1L) can suppress the toxicity associated with HttQ120 (Warrick et al., 1999). Similarly, introduction of HSPA1L into *trpml* neurons, but not in other cell types, rescued the mutant phenotypes. This finding indicates that the impairments in *trpml* arose primarily in neurons and possibly due to an accumulation of macromolecules.

Model for Motor Defects due to Loss of TRPML

Loss of TRPML causes a decrease in lysosomal degradation, resulting in an increase in dysfunctional mitochondria, aggregation of toxic macromolecules, and oxidative stress. Lipofuscin, which forms under oxidative stress (Terman and Brunk, 2004), can cause a further decrease in lysosomal function. We propose that, in *trpml* mutants, there is an amplifying cycle of increased oxidative stress and defective autophagy and lysosomal function, which leads to progressive neurodegeneration and motor impairment. We suggest that elevated oxidative stress also underlies the reduced NMJ synaptic transmission in *trpml* animals, which in turn contributes to the deficit in behavioral motor function. Consistent with this model, increased oxidative stress is linked to inhibition of synaptic transmission (Giniatullin et al., 2006). Our results raise the possibility that a combination of neurodegeneration and loss of NMJ synaptic transmission accounts for the diminished motor activity in MLIV patients. Although we cannot rule out that the impaired synaptic transmission in *trpml* is an indirect consequence of unhealthy neurons, it still provides an explanation for the impaired motor function that precedes neurodegeneration in MLIV.

The *trpml* phenotype is reminiscent of the *spinster/benchwarmer Drosophila* mutant. Similarities include accumulation of lipofuscin-loaded effete lysosomes, loss of NMJ synaptic function, and neurodegeneration (Nakano et al., 2001; Sweeney and Davis, 2002; Dermaut et al., 2005). The Spinster/Benchwarmer protein also resides in a presynaptic lysosomal compartment and is implicated in efficient SV recycling (Sweeney and Davis, 2002; Dermaut et al., 2005).

TRPML Is Required in Hematopoietic Cells and Glia to Mediate Clearance of Apoptotic Cells and to Prevent Widespread Neurodegeneration

Initially, as a control, we introduced the wild-type *trpml*$^+$ transgene in glia and fat bodies/hemocytes and, to our surprise, expression of *trpml*$^+$ in these cells rescued the *trpml* mutant phenotypes. Thus, the issue arises as to why expression of TRPML in hematopoietic cells or glia rescues the *trpml* defects. Clarifying this mechanism may have relevance to other LSD models of progressive neurodegeneration, since reintroduction of *Drosophila* NPC1 in glia reduces adult lethality associated with the *dnpc1a* mutation (Phillips et al., 2008).

Neural tissue in *trpml* animals accumulates early- and late-apoptotic/necrotic cells. Normally, early-apoptotic cells are rapidly cleared by hemocytes and glia (Wood and Jacinto, 2007). If dead cells are not cleared rapidly, they lose plasma membrane integrity and release antigenic and cytotoxic materials, which induce neuroinflammation and secondary necrosis in neighboring bystander cells (Franc, 2002). Loss of *trpml* function in neurons induces cell-autonomous apoptosis, and defective clearance of these cells induces secondary cell death in nearby cells. Consistent with this proposal, introduction of *trpml*$^+$ in neurons prevents cell death of both neurons and glia, indicating that *trpml* functions cell autonomously for neuronal viability and nonautonomously for the viability of adjacent cells, such as glia. When *trpml* was introduced in hemocytes or glia, there was no accumulation of late-apoptotic cells or necrotic cells, although mutant cells still underwent early apoptosis.

We suggest that expression of *trpml*$^+$ in hemocytes and glia promotes the clearance of early-apoptotic cells before their membrane integrity is compromised. In the absence of this function, there is an accumulation of late-apoptotic/necrotic cells, leading to widespread neuroinflammation and progressive cell death in adjoining cells that would otherwise remain unaffected.

Since both late-apoptotic/necrotic neurons and oxidative stress are mediators of neuroinflammation (Franc, 2002), our results raise the possibility that neuroinflammation may be a hitherto unexplored mediator of MLIV associated neurodegeneration. This is, to our knowledge, the first link between a TRP channel and either neuroinflammation or clearance of apoptotic cells.

Development of Therapeutic Strategies

The finding that expression of wild-type *trpml*$^+$ in hematopoietic cells is sufficient to delay the onset of the *trpml* mutant phenotypes raises the exciting possibility that bone marrow transplantation (BMT) in patients with MLIV might delay disease progression. In favor of this proposal, several reports and case studies describe the successful use of BMT to ameliorate other LSDs in patients and in murine models (Bruni et al., 2007). With the recent development of TRPML1 knockout mice (Venugopal et al., 2007), the feasibility of this approach can now be tested in a mammalian animal model. Our results also raise the possibility that one or more of the approved drugs that stimulate either autophagy or HSP1AL may also suppress MLIV, especially in combination with BMT. Thus, this *Drosophila* model for MLIV provides the framework for developing strategies to treat MLIV.

EXPERIMENTAL PROCEDURES

Generation of Transgenic and Mutant *trpml* Strains

trpml^1 and *trpml*^{2} were generated by imprecise excision of the *P* element (GE22279). The deletions in *trpml*^{1} and *trpml*^{2} removed −456 to +641 and −234 to +860 base pairs, respectively, relative to the translation start site. P[*trpml*] was generated by cloning the region between the genes *Gyc76C* and *CG32209* into pCaSpeR. The *UAS-trpml* transgenic flies were generated by subcloning the *trpml* cDNA into pUAST. Other strains are described in the Supplemental Experimental Procedures.

Locomotor Activity Assays

A total of 10–20 flies were placed in a 50 ml graduated cylinder. The climbing index was the fraction of flies that climbed to the 25 ml mark within 15 s after being tapped down. Total daily activity was determined by placing individual flies in a DAMS actometer (Trikinetics) for 24 hr. Animals were not exposed to CO_2 for $\geq$ 24 hr prior to performing the assays.

Assays for Apoptosis

Brains were dissected from flies immediately after removing the heads from live flies to prevent necrosis due to hypoxia. TUNEL staining was performed as described by the manufacturer, Roche. PI staining (1:3000 dilution in PBS) was performed for 10 min. To determine the types of cells dying, brains were dissected, stained with antibodies that label neurons or glia, followed by TUNEL staining as described in the Supplemental Experimental Procedures. Images were viewed by confocal microscopy.

Light Microscopy and Transmission EM

Heads were dissected from flies reared under a 12 hr light/dark cycle or constant darkness, and embedded as previously described (Porter et al., 1992), except that 0.1 M sodium phosphate (pH 7.4) was the buffer. For light microscopy, 1 μm sections were prepared (50–100 μm depth), stained with 1% toluidine blue, and viewed by light microscopy. For transmission EM, 85 nm sections were prepared at a depth of 30 μm.

Cytoplasmic membrane inclusions and autophagosomes were evaluated in photoreceptor cell bodies. Vesicles were characterized as multilamellar or multivesicular bodies based on established morphological criteria (Dermaut et al., 2005). The numbers of cytoplasmic inclusions per photoreceptor cell body were counted in $\geq$50 ommatidia per fly (n $\geq$ 3 flies).

Detection of GFP-ATG8

Wild-type and *trpml*^{1} flies containing the *hsGFP-ATG8* transgene were heat shocked for 1 hr at 37°C 48 hr prior to performing experiments. Brains were dissected and imaged as described above. For the quantification of GFP-ATG8 positive vesicles, ommatidia were dissected as described above from a set of six flies per experiment (n $\geq$ 3). Sections (1 μm) spanning the entire ommatidia (thickness of 10–12 μm on the coverslips) were obtained by confocal microscopy and projected into a single image. The total numbers of GFP-positive vesicles per ommatidia were determined for the quantification of the GFP-ATG8 puncta.

Detection of Rh1 Degradation

Flies were exposed to either ambient or blue (480 nm) light for 6 hr before dissecting heads under a photographic safelight. Heads were homogenized in SDS-sample buffer. Proteins were fractionated by SDS-PAGE, transferred to nitrocellulose, and probed with mouse anti-Rh1 and rabbit anti-TRP antibodies and with anti-rabbit IRDye 800 CW and anti-mouse IRDye 680 conjugates (Odyssey). Signals were detected and quantified using a LICOR imaging system (Odyssey).

MitoTracker Staining

Ommatidia were dissected, loaded with MitoTracker-orange CM-H2TMRos (100 nM; Invitrogen) for 30 min, fixed for 15 min in 4% PFA, washed, mounted, and imaged as described above.

TEVC Recordings and FM1-43 Imaging

Recordings were performed on third instar NMJ using TEVC previously described techniques (Rohrbough et al., 1999). Optical FM1-43 dye imaging was performed at the NMJ as previously described (Trotta et al., 2004) (Supplemental Experimental Procedures).

Measurement of H_2O_2 Levels

Ten flies were homogenized in PBS, incubated at 4°C for 15 min, the extracts centrifuged, and the supernatants retained. H_2O_2 levels were measured using the Amplex-red H_2O_2 kit (Invitrogen) using a Fluorstar Optima fluorescent plate reader (BMG). Samples without fly extracts were used to determine backgrounds.

Optical Neutralization Technique

To assay the time course of photoreceptor cell degeneration, the numbers of rhabdomeres/ommatidium were determined as previously described (Xu et al., 2004). Each data point was based on $\geq$50 ommatidia per fly (n $\geq$ 3 flies).

Statistics

All statistical values indicate means ± SEM. We used ANOVA to make multi-group comparisons and Student's t tests to compare two sets of values.

SUPPLEMENTAL DATA

Supplemental Data include Supplemental Experimental Procedures and eight figures and are available with this article online at http://www.cell.com/supplemental/S0092-8674(08)01198-7.

ACKNOWLEDGMENTS

We thank the Bloomington Stock Center for fly stocks, T. Neufeld for the *hsGFP-ATG8* flies, N. Franc for the *UAS-crq* flies, J. Corden, J. Lorsch, R. Rao, and S. Muend for use of equipment, and M. Sepanski for preparing sections of fly heads. We thank S.J. Moon, Y. Jiao, and X. Wang for technical advice, and M. Köttgen, Y. Kwon, and D. Wasserman for helpful discussions. We also thank the Microscopy Facility at the Cell Biology Department, the Johns Hopkins University School of Medicine, for use of their equipment. K.V. was supported in part by an MLIV Foundation postdoctoral fellowship. The work in the K.B. laboratory was supported by the National Institute of Neurological Disorders and Stroke (NS41740), and that in the C.M. laboratory was supported by grants from the March of Dimes and the National Eye Institute (EY08117). The authors declare no conflicts of interest.

Received: January 15, 2008
Revised: July 25, 2008
Accepted: September 17, 2008
Published: November 26, 2008

REFERENCES

Awasaki, T., Tatsumi, R., Takahashi, K., Arai, K., Nakanishi, Y., Ueda, R., and Ito, K. (2006). Essential role of the apoptotic cell engulfment genes *draper* and *ced-6* in programmed axon pruning during *Drosophila* metamorphosis. Neuron *50*, 855–867.

Bach, G. (2005). Mucolipin 1: endocytosis and cation channel-a review. Pflugers Arch. *451*, 313–317.

Badre, N.H., Martin, M.E., and Cooper, R.L. (2005). The physiological and behavioral effects of carbon dioxide on *Drosophila melanogaster* larvae. Comp. Biochem. Physiol. A Mol. Integr. Physiol. *140*, 363–376.

Bargal, R., Avidan, N., Ben-Asher, E., Olender, Z., Zeigler, M., Frumkin, A., Raas-Rothschild, A., Glusman, G., Lancet, D., and Bach, G. (2000). Identification of the gene causing mucolipidosis type IV. Nat. Genet. *26*, 118–123.

Bassi, M.T., Manzoni, M., Monti, E., Pizzo, M.T., Ballabio, A., and Borsani, G. (2000). Cloning of the gene encoding a novel integral membrane protein, mucolipidin-and identification of the two major founder mutations causing mucolipidosis type IV. Am. J. Hum. Genet. *67*, 1110–1120.

Brignull, H.R., Morley, J.F., and Morimoto, R.I. (2007). The stress of misfolded proteins: *C. elegans* models for neurodegenerative disease and aging. Adv. Exp. Med. Biol. *594*, 167–189.

Bruni, S., Loschi, L., Incerti, C., Gabrielli, O., and Coppa, G.V. (2007). Update on treatment of lysosomal storage diseases. Acta Myol. *26*, 87–92.

Cooper, J.D. (2003). Progress towards understanding the neurobiology of Batten disease or neuronal ceroid lipofuscinosis. Curr. Opin. Neurol. *16*, 121–128.

Dermaut, B., Norga, K.K., Kania, A., Verstreken, P., Pan, H., Zhou, Y., Callaerts, P., and Bellen, H.J. (2005). Aberrant lysosomal carbohydrate storage accompanies endocytic defects and neurodegeneration in *Drosophila benchwarmer*. J. Cell Biol. *170*, 127–139.

Deshmukh, M., Kuida, K., and Johnson, E.M., Jr. (2000). Caspase inhibition extends the commitment to neuronal death beyond cytochrome c release to the point of mitochondrial depolarization. J. Cell Biol. *150*, 131–143.

Fares, H., and Greenwald, I. (2001). Regulation of endocytosis by CUP-5, the *Caenorhabditis elegans* mucolipin-1 homolog. Nat. Genet. *28*, 64–68.

Fergestad, T., and Broadie, K. (2001). Interaction of stoned and synaptotagmin in synaptic vesicle endocytosis. J. Neurosci. *21*, 1218–1227.

Fletcher, B.L., Dillard, C.J., and Tappel, A.L. (1973). Measurement of fluorescent lipid peroxidation products in biological systems and tissues. Anal. Biochem. *52*, 1–9.

Franc, N.C. (2002). Phagocytosis of apoptotic cells in mammals, *Caenorhabditis elegans* and *Drosophila* melanogaster: molecular mechanisms and physiological consequences. Front. Biosci. *7*, d1298–d1313.

Franc, N.C., Dimarcq, J.L., Lagueux, M., Hoffmann, J., and Ezekowitz, R.A. (1996). Croquemort, a novel *Drosophila* hemocyte/macrophage receptor that recognizes apoptotic cells. Immunity *4*, 431–443.

Franc, N.C., Heitzler, P., Ezekowitz, R.A., and White, K. (1999). Requirement for croquemort in phagocytosis of apoptotic cells in *Drosophila*. Science *284*, 1991–1994.

Giniatullin, A.R., Darios, F., Shakirzyanova, A., Davletov, B., and Giniatullin, R. (2006). SNAP25 is a pre-synaptic target for the depressant action of reactive oxygen species on transmitter release. J. Neurochem. *98*, 1789–1797.

Goldin, E., Blanchette-Mackie, E.J., Dwyer, N.K., Pentchev, P.G., and Brady, R.O. (1995). Cultured skin fibroblasts derived from patients with mucolipidosis 4 are auto-fluorescent. Pediatr. Res. *37*, 687–692.

Hersh, B.M., Hartwieg, E., and Horvitz, H.R. (2002). The *Caenorhabditis elegans* mucolipin-like gene *cup-5* is essential for viability and regulates lysosomes in multiple cell types. Proc. Natl. Acad. Sci. USA *99*, 4355–4360.

Jennings, J.J., Jr., Zhu, J.H., Rbaibi, Y., Luo, X., Chu, C.T., and Kiselyov, K. (2006). Mitochondrial aberrations in mucolipidosis Type IV. J. Biol. Chem. *281*, 39041–39050.

Klionsky, D.J. (2007). Autophagy: from phenomenology to molecular understanding in less than a decade. Nat. Rev. Mol. Cell Biol. *8*, 931–937.

Kretzschmar, D., Hasan, G., Sharma, S., Heisenberg, M., and Benzer, S. (1997). The *swiss cheese* mutant causes glial hyperwrapping and brain degeneration in *Drosophila*. J. Neurosci. *17*, 7425–7432.

Kuromi, H., and Kidokoro, Y. (2000). Tetanic stimulation recruits vesicles from reserve pool via a cAMP-mediated process in *Drosophila* synapses. Neuron *27*, 133–143.

Lee, C.Y., and Baehrecke, E.H. (2001). Steroid regulation of autophagic programmed cell death during development. Development *128*, 1443–1455.

Li, J., Huang, C.Y., Zheng, R.L., Cui, K.R., and Li, J.F. (2000). Hydrogen peroxide induces apoptosis in human hepatoma cells and alters cell redox status. Cell Biol. Int. *24*, 9–23.

Manzoni, M., Monti, E., Bresciani, R., Bozzato, A., Barlati, S., Bassi, M.T., and Borsani, G. (2004). Overexpression of wild-type and mutant mucolipin proteins in mammalian cells: effects on the late endocytic compartment organization. FEBS Lett. *567*, 219–224.

Ménoret, A., Chaillot, D., Callahan, M., and Jacquin, C. (2002). Hsp70, an immunological actor playing with the intracellular self under oxidative stress. Int. J. Hyperthermia *18*, 490–505.

Miedel, M.T., Rbaibi, Y., Guerriero, C.J., Colletti, G., Weixel, K.M., Weisz, O.A., and Kiselyov, K. (2008). Membrane traffic and turnover in TRP-ML1-deficient cells: a revised model for mucolipidosis type IV pathogenesis. J. Exp. Med. *205*, 1477–1490.

Mizushima, N. (2004). Methods for monitoring autophagy. Int. J. Biochem. Cell Biol. *36*, 2491–2502.

Nakano, Y., Fujitani, K., Kurihara, J., Ragan, J., Usui-Aoki, K., Shimoda, L., Lukacsovich, T., Suzuki, K., Sezaki, M., Sano, Y., et al. (2001). Mutations in the novel membrane protein spinster interfere with programmed cell death and cause neural degeneration in *Drosophila melanogaster*. Mol. Cell. Biol. *21*, 3775–3788.

Pang, Z., and Geddes, J.W. (1997). Mechanisms of cell death induced by the mitochondrial toxin 3-nitropropionic acid: acute excitotoxic necrosis and delayed apoptosis. J. Neurosci. *17*, 3064–3073.

Phillips, S.E., Woodruff, E.A., 3rd, Liang, P., Patten, M., and Broadie, K. (2008). Neuronal loss of *Drosophila* NPC1a causes cholesterol aggregation and age-progressive neurodegeneration. J. Neurosci. *28*, 6569–6582.

Porter, J.A., Hicks, J.L., Williams, D.S., and Montell, C. (1992). Differential localizations of and requirements for the two *Drosophila* ninaC kinase/myosins in photoreceptor cells. J. Cell Biol. *116*, 683–693.

Ravikumar, B., Vacher, C., Berger, Z., Davies, J.E., Luo, S., Oroz, L.G., Scaravilli, F., Easton, D.F., Duden, R., O'Kane, C.J., et al. (2004). Inhibition of mTOR induces autophagy and reduces toxicity of polyglutamine expansions in fly and mouse models of Huntington disease. Nat. Genet. *36*, 585–595.

Rohrbough, J., Pinto, S., Mihalek, R.M., Tully, T., and Broadie, K. (1999). latheo, a *Drosophila* gene involved in learning, regulates functional synaptic plasticity. Neuron *23*, 55–70.

Scott, R.C., Schuldiner, O., and Neufeld, T.P. (2004). Role and regulation of starvation-induced autophagy in the *Drosophila* fat body. Dev. Cell *7*, 167–178.

Settembre, C., Fraldi, A., Rubinsztein, D.C., and Ballabio, A. (2007). Lysosomal storage diseases as disorders of autophagy. Autophagy *4*, 113–114.

Soyombo, A.A., Tjon-Kon-Sang, S., Rbaibi, Y., Bashllari, E., Bisceglia, J., Muallem, S., and Kiselyov, K. (2006). TRP-ML1 regulates lysosomal pH and acidic lysosomal lipid hydrolytic activity. J. Biol. Chem. *281*, 7294–7301.

St.-Pierre, J., Drori, S., Uldry, M., Silvaggi, J.M., Rhee, J., Jager, S., Handschin, C., Zheng, K., Lin, J., Yang, W., et al. (2006). Suppression of reactive oxygen species and neurodegeneration by the PGC-1 transcriptional coactivators. Cell *127*, 397–408.

Sun, M., Goldin, E., Stahl, S., Falardeau, J.L., Kennedy, J.C., Acierno, J.S., Jr., Bove, C., Kaneski, C.R., Nagle, J., Bromley, M.C., et al. (2000). Mucolipidosis type IV is caused by mutations in a gene encoding a novel transient receptor potential channel. Hum. Mol. Genet. *9*, 2471–2478.

Sweeney, S.T., and Davis, G.W. (2002). Unrestricted synaptic growth in *spinster*-a late endosomal protein implicated in TGF-β-mediated synaptic growth regulation. Neuron *36*, 403–416.

Terman, A., and Brunk, U.T. (2004). Lipofuscin. Int. J. Biochem. Cell Biol. *36*, 1400–1404.

Trotta, N., Rodesch, C.K., Fergestad, T., and Broadie, K. (2004). Cellular bases of activity-dependent paralysis in *Drosophila* stress-sensitive mutants. J. Neurobiol. *60*, 328–347.

Twig, G., Elorza, A., Molina, A.J., Mohamed, H., Wikstrom, J.D., Walzer, G., Stiles, L., Haigh, S.E., Katz, S., Las, G., et al. (2008). Fission and selective fusion govern mitochondrial segregation and elimination by autophagy. EMBO J. *27*, 433–446.

van den Eijnde, S.M., Boshart, L., Baehrecke, E.H., De Zeeuw, C.I., Reutelingsperger, C.P., and Vermeij-Keers, C. (1998). Cell surface exposure of phosphatidylserine during apoptosis is phylogenetically conserved. Apoptosis *3*, 9–16.

Venkatachalam, K., Hofmann, T., and Montell, C. (2006). Lysosomal localization of TRPML3 depends on TRPML2 and the mucolipidosis-associated protein TRPML1. J. Biol. Chem. *281*, 17517–17527.

Venkatachalam, K., and Montell, C. (2007). TRP channels. Annu. Rev. Biochem. *76*, 387–417.

Venugopal, B., Browning, M.F., Curcio-Morelli, C., Varro, A., Michaud, N., Nanthakumar, N., Walkley, S.U., Pickel, J., and Slaugenhaupt, S.A. (2007). Neurologic, gastric, and opthalmologic pathologies in a murine model of mucolipidosis type IV. Am. J. Hum. Genet. *81*, 1070–1083.

Wang, T., and Montell, C. (2007). Phototransduction and retinal degeneration in *Drosophila*. Pflügers Arch. *454*, 821–847.

Warrick, J.M., Chan, H.Y., Gray-Board, G.L., Chai, Y., Paulson, H.L., and Bonini, N.M. (1999). Suppression of polyglutamine-mediated neurodegeneration in *Drosophila* by the molecular chaperone HSP70. Nat. Genet. *23*, 425–428.

Wood, W., and Jacinto, A. (2007). *Drosophila* melanogaster embryonic haemocytes: masters of multitasking. Nat. Rev. Mol. Cell Biol. *8*, 542–551.

Xu, H., Lee, S.J., Suzuki, E., Dugan, K.D., Stoddard, A., Li, H.S., Chodosh, L.A., and Montell, C. (2004). A lysosomal tetraspanin associated with retinal degeneration identified via a genome-wide screen. EMBO J. *23*, 811–822.